Geochemical Perspectives Letters

Early differentiation of magmatic iron meteorite parent bodies from Mn–Cr chronometry

A. Anand[1*], J. Pape[1,2], M. Wille[1], K. Mezger[1], B. Hofmann[1,3]

OPEN ACCESS

https://doi.org/10.7185/geochemlet.2136

Abstract

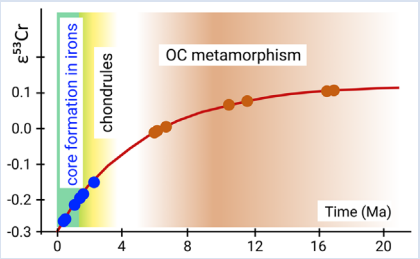

Magmatic iron meteorite groups such as IIAB, IIIAB and IVA, represent the largest sampling of extraterrestrial core material from the earliest accreted distinct planetary bodies in the solar system. Chromium isotope compositions of chromite/daubréelite from seven samples, translated into $^{53}Cr/^{52}Cr$ model ages, provide robust time information on planetary core formation. These ages are within ~1.5 Ma after formation of calcium-aluminium-rich inclusions (CAIs) and define the time of metal core formation in the respective parent bodies, assuming metal–silicate separation was an instantaneous event that induced strong chemical fractionation of Mn from the more siderophile Cr. The early core formation ages support accretion and differentiation of the magmatic iron meteorite parent bodies to have occurred prior to the chondrule formation interval. The calibration of Mn–Cr ages with established Hf–W ages of samples from the same magmatic iron meteorite groups constrains the initial $\varepsilon^{53}Cr$ of the solar system to -0.30 ± 0.05, and thus lower than previously estimated.

Received 5 August 2021 | Accepted 17 November 2021 | Published 13 December 2021

Introduction

Members of the different magmatic iron meteorite groups are thought to sample the cores of distinct parent bodies that experienced large scale chemical fractionation, most notably metal–silicate separation. The absolute time of core formation provides a key time marker for the evolution of early formed planetesimals including accretion and cooling of the respective parent body. The most commonly used chronological system to date iron meteorites is the $^{182}Hf–^{182}W$ system (Kruijer *et al.*, 2017 and references therein), constraining core formation in iron meteorite parent bodies over an interval of ~1 Myr and their accretion to ~0.1–0.3 Ma after the formation of Ca-Al-rich inclusions (4567.18 ± 0.50 Ma; Amelin *et al.*, 2010). These early accretion ages predate or are contemporaneous with the chondrule formation interval (*e.g.*, Connelly *et al.*, 2012; Pape *et al.*, 2019). However, correct interpretation of Hf–W data depends on the accurate knowledge of initial $\varepsilon^{182}W$ of the solar system and Hf/W ratios of the parent bodies which are well established but still needs to consider possible variations in Hf isotopes due to galactic cosmic radiation (GCR) (Kruijer *et al.*, 2017).

Another powerful tool to constrain the time and duration of early solar system processes, including accretion, differentiation, metamorphism and subsequent cooling could be the short lived $^{53}Mn–^{53}Cr$ chronometer ($t_{1/2} = 3.7 \pm 0.4$ Ma; Honda and Imamura, 1971) (*e.g.*, Shukolyukov and Lugmair, 2006; Trinquier *et al.*, 2008; Göpel *et al.*, 2015; Zhu *et al.*, 2021). Chromite ($FeCr_2O_4$) and daubréelite ($FeCr_2S_4$) are the two main carrier phases of Cr in magmatic iron meteorites. Both minerals have low Mn/Cr ratios (≤0.01; Duan and Regelous, 2014) and thus preserve the Cr isotope composition of their growth environment at the time of isotopic closure, while the in-growth of radiogenic ^{53}Cr from *in situ* decay of ^{53}Mn is negligible (Anand *et al.*, 2021). This makes them suitable for obtaining model ages by comparing their Cr isotopic composition with the Cr isotope evolution of the host reservoir. A particular advantage is that low Fe/Cr ratios in chromite and daubréelite (typically ~0.5) result in negligible contribution of ^{53}Cr produced by GCR from Fe; hence no correction for spallogenic Cr is required (Trinquier *et al.*, 2008; Liu *et al.*, 2019) (Supplementary Information).

This study presents model ages for chromite and daubréelite from the largest magmatic iron meteorite group collections (IIAB, IIIAB and IVA) that constrain the earliest stages of planetesimal formation and differentiation. These Cr model ages define the timing of metal segregation during core formation. Chromium-rich phases formed in the metal inherit the Cr isotope composition of their low Mn/Cr host and thus constrain the time of last silicate–metal equilibration.

Methods

A chromite or daubréelite fraction from seven iron meteorites was analysed. After mineral digestion and chemical purification, Cr isotopes were measured on a Triton™ Plus TIMS at the University of Bern. Each sample was measured on multiple filaments to achieve high precision for $^{53}Cr/^{52}Cr$ ratio. Isotope compositions are reported as parts *per* 10,000 deviations (ε notation) from the mean

1. Institut für Geologie, Universität Bern, Baltzerstrasse 1+3, 3012 Bern, Switzerland
2. Institut für Planetologie, Universität Münster, Wilhelm-Klemm-Str. 10, 48149 Münster, Germany
3. Naturhistorisches Museum Bern, Bernastrasse 15, CH-3005, Bern, Switzerland
* Corresponding author (email: aryavart.anand@geo.unibe.ch)

value of a terrestrial Cr standard measured along with the samples in each session. External precision (2 s.d.) for the terrestrial standard in a typical measurement session was ±0.1 for ε^{53}Cr and ±0.2 for ε^{54}Cr (Supplementary Information).

Model for ε^{53}Cr evolution in chondritic reservoir. Model ^{53}Cr/^{52}Cr ages for early formed solar system bodies and their components can be determined on materials with high Cr/Mn and considering the following (i) homogeneous distribution of ^{53}Mn in the solar system (*e.g.*, Trinquier *et al.*, 2008; Zhu *et al.*, 2019), (ii) known abundances of ^{53}Mn and ^{53}Cr at the beginning of the solar system (*i.e.* solar system initial ε^{53}Cr) or any point in time thereafter, (iii) an estimate for the Mn/Cr in the relevant reservoir, and (iv) known decay constant of ^{53}Mn. Based on these assumptions the evolution of the ^{53}Cr/^{52}Cr isotope composition of the chondritic reservoir through time can be expressed as:

$$\left(^{53}\mathrm{Cr}/^{52}\mathrm{Cr}\right)_{\mathrm{p}} = \left(^{53}\mathrm{Cr}/^{52}\mathrm{Cr}\right)_{\mathrm{i}} + (k)\left(^{53}\mathrm{Mn}/^{55}\mathrm{Mn}\right)_{\mathrm{i}} \times \left(1 - e^{-\lambda t}\right) \quad \text{Eq. 1}$$

where the subscripts 'p' and 'i' refer to the present day and initial solar system values, respectively, and λ denotes the ^{53}Mn decay constant. The ^{55}Mn/^{52}Cr of the reservoir is denoted by k; and t represents the time elapsed since the start of the solar system, which is equated with the time of formation of CAIs. Equation 1 describes the evolution of ^{53}Cr/^{52}Cr with time for the chondritic reservoir and can be used to derive model ages for a meteorite sample by measuring the Cr isotopic composition of its chromite/daubréelite fraction.

Results

The ε^{53}Cr and ε^{54}Cr of chromite/daubréelite fractions determined for all samples are listed in Table 1. No correlation is observed in ε^{53}Cr *vs.* ε^{54}Cr and ε^{53}Cr *vs.* Fe/Cr that corroborates an insignificant spallogenic contribution (Supplementary Information). Model ages are calculated relative to the CAI formation age of 4567.18 ± 0.50 Ma (Amelin *et al.*, 2010) assuming an OC chondritic ^{55}Mn/^{52}Cr = 0.74 (Zhu *et al.*, 2021), a solar system initial ε^{53}Cr = −0.23 and a canonical ^{53}Mn/^{55}Mn = 6.28×10^{-6} (Trinquier *et al.*, 2008) (Fig. 1).

Discussion

The inference of Mn–Cr model ages to date core formation events is based on the assumption that metal–silicate separation was instantaneous. It occurred when the chondritic parent bodies of magmatic iron meteorites were heated by accretion energy and the decay of short lived ^{26}Al, and reached the liquidus temperature of iron–sulfur alloy (1325 °C to 1615 °C, depending on the S content in the metal melt; Kaminski *et al.*, 2020 and references therein). The metal–silicate separation induced a strong chemical fractionation of Mn from the more siderophile Cr (Mann *et al.*, 2009). The measured low Mn/Cr (≤0.01; Duan and Regelous, 2014) in iron meteorites corroborates the efficiency of this fractionation. Because of the low Mn/Cr of the metallic core, its Cr isotopic composition remained unchanged and reflects the composition at the time of metal–silicate differentiation. Therefore, the Cr isotopic composition of chromite/daubréelite that formed in the metallic core, no matter at what time after the metal segregation, reflects the time of Mn/Cr fractionation from a reservoir with CI chondritic ^{55}Mn/^{52}Cr and not the time of mineral formation nor its closure below a certain closure temperature.

The Mn–Cr model ages determined using Equation 1. assume a Mn/Cr for the source reservoir that is represented by the average Mn/Cr of OCs. Ordinary chondrites have a CI-like Mn/Cr (*e.g.*, Wasson and Allemeyn, 1988; Zhu *et al.*, 2021) and alongside the investigated magmatic iron meteorite groups, belong to the 'non-carbonaceous' reservoir (Kleine *et al.*, 2020). The effect of different Mn/Cr of the iron meteorite parent bodies and the assumption of different initial ε^{53}Cr is shown in Figure S-2. Model ages for IIAB, IIIAB and IVA groups are unaffected by the growth trajectory chosen, given current analytical resolution. Assuming a Mn/Cr similar to carbonaceous chondrites would change the model ages by a maximum of 1 Ma for the youngest sample. However, since all samples belong to the non-carbonaceous group, the average composition of OCs is most appropriate.

Since the Cr isotopic composition of the samples is unaffected by contributions from spallogenic Cr (Supplementary Information), the only major source of uncertainty in Mn–Cr model ages comes from the choice of initial ε^{53}Cr and ^{53}Mn/^{55}Mn values. Figure S-3 shows Mn–Cr model ages for the studied samples determined using initial Mn–Cr isotopic compositions from multiple studies reporting resolvable variations in the solar system initial ε^{53}Cr and ^{53}Mn/^{55}Mn values. Clearly, more high precision Cr isotope data for samples dated with different chronometers are needed to further constrain the initial ε^{53}Cr and ^{53}Mn/^{55}Mn. Model ages determined using initial ε^{53}Cr and ^{53}Mn/^{55}Mn values from Göpel *et al.* (2015) and Shukolyukov and Lugmair (2006) predate the CAI formation

Table 1 Mn/Cr, Fe/Cr and Cr isotopic compositions of chromite and daubréelite fractions from iron meteorites.

Sample (Coll. Number)	Group/Fraction	Mn/Cr	Fe/Cr	ε^{53}Cr	2 s.e.	ε^{54}Cr	2 s.e.	Model Age[a]	Model Age[b]	*n*
Agoudal (43830)	IIAB/Chromite	0.0053(4)	0.37(1)	−0.210	0.023	−0.784	0.060	$0.27^{+0.33}_{-0.31}$	$1.33^{+0.41}_{-0.38}$	12
Sikhote Alin (43380)	IIAB/Chromite	0.0052(8)	0.41(3)	−0.228	0.025	−0.923	0.051	$0.03^{+0.34}_{-0.32}$	$1.04^{+0.41}_{-0.38}$	12
NWA 11420 (43837)	IIAB/Daubréelite	0.0040(1)	0.59(1)	−0.203	0.045	−0.768	0.055	$0.37^{+0.67}_{-0.59}$	$1.45^{+0.83}_{-0.72}$	7
Saint Aubin[c]	IIIAB/Chromite	0.0096(2)	0.57(1)	−0.268	0.029	−0.779	0.061	$-0.47^{+0.35}_{-0.33}$	$0.44^{+0.42}_{-0.39}$	10
Cape York (33137)	IIIAB/Chromite	0.0062(3)	0.46(1)	−0.196	0.043	−0.780	0.062	$0.47^{+0.64}_{-0.57}$	$1.57^{+0.80}_{-0.70}$	13
Yanhuitlan (50084)	IVA/Daubréelite	0.0490(7)	0.54(1)	−0.272	0.027	−0.468	0.061	$-0.52^{+0.33}_{-0.31}$	$0.38^{+0.39}_{-0.36}$	10
Duchesne (50033)	IVA/Chromite	0.0048(4)	1.1(1)	−0.160	0.037	−0.487	0.156	$1.00^{+0.61}_{-0.55}$	$2.23^{+0.78}_{-0.68}$	7
IAG OKUM	whole rock std.	0.60(6)	36.6(9)	+0.020	0.065	+0.083	0.110			7

Collection numbers refer to meteorite collections of NHM Bern.
The uncertainties associated with Mn/Cr, Fe/Cr, and Cr isotopic compositions are reported as 2 s.e. of the replicate measurements. See Table S-1 for Cr isotopic composition of the individual runs. *n* = number of replicate measurements.
[a] Equation 1, $\varepsilon^{53}\mathrm{Cr_i} = -0.23$.
[b] Equation 1, $\varepsilon^{53}\mathrm{Cr_i} = -0.30$.
[c] NHM Vienna collection ID for Saint Aubin: NHMV_#13635_[A].

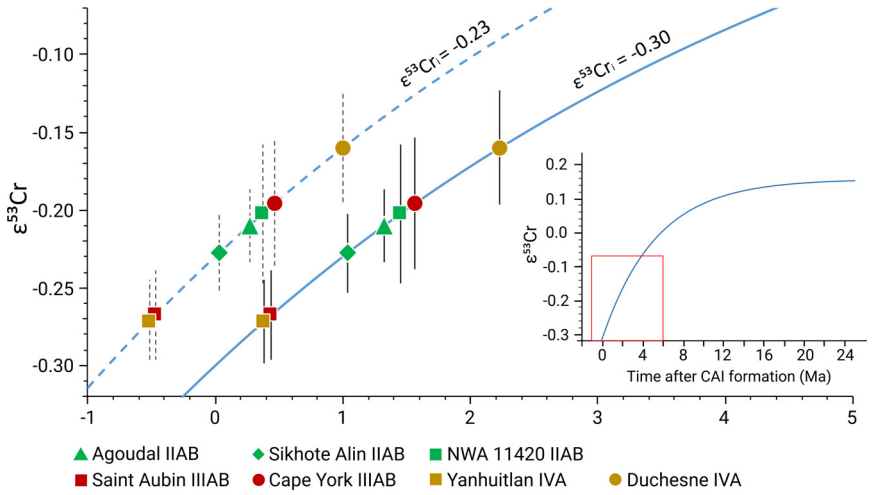

Figure 1 ε^{53}Cr values of chromite/daubréelite plotted on a Cr isotope evolution curve determined for a chondritic reservoir through time using Equation 1. Error bars represent 2 s.e. uncertainties.

age, contradicting the standard solar system model in which CAIs are the earliest formed solid objects. The Mn–Cr model ages determined using initial ε^{53}Cr and ^{53}Mn/^{55}Mn from Trinquier *et al.* (2008) mostly postdate CAI formation and thus appear generally more reliable.

The Mn–Cr model ages can also be compared with other chronometers that have been used to date meteorites and their components. ^{182}Hf–^{182}W, ^{207}Pb–^{206}Pb and ^{187}Re–^{187}Os are some of the common chronological systems providing constraints on different stages in the evolution of iron meteorite parent bodies (Goldstein *et al.*, 2009 and references therein). However, when applied to iron meteorites all other chronological systems date cooling below their respective isotopic closure with the exception of the ^{182}Hf–^{182}W system, which has strong similarities to the ^{53}Mn–^{53}Cr system. It is also suitable for examining the timescales and mechanisms of metal segregation for iron meteorite parent bodies since Hf and W have different geochemical behaviours resulting in strong Hf/W fractionation during metal/silicate separation (*i.e.* core formation). However, in addition to the uncertainty on the initial ε^{182}W of the solar system, ^{182}W/^{184}W data are also affected by secondary neutron capture effects on W isotopes induced during cosmic ray exposure (unlike Mn–Cr model ages reported here). Recently, Pt isotope data have been used to quantify the effects of neutron capture on W isotope compositions, making it possible to produce more reliable core formation ages (*e.g.*, Kruijer *et al.*, 2017). The Mn–Cr core formation age corresponding to the weighted mean ε^{53}Cr of combined IIAB, IIIAB and IVA groups determined using solar system initial ε^{53}Cr = −0.23 (Trinquier *et al.*, 2008) is ~1 Myr older than the Hf–W core formation age corresponding to Pt corrected weighted mean ε^{182}W of the same iron groups (Fig. 2, Table S-2) (Kruijer *et al.*, 2017). However, the Hf–W and Mn–Cr systems show consistent crystallisation ages in angrites (internal isochrons established by minerals) that also belong to the 'non-carbonaceous' reservoir and originated from differentiated parent bodies (Zhu *et al.*, 2019). The different chronometers are expected to agree because of the rapid cooling of angrites indicated by their basaltic texture. A better fit between Hf–W and Cr model ages can be obtained when the uncertainties on the model parameters for Mn–Cr model age determination are considered. Uncertainties on the ^{53}Mn decay constant (Honda and Imamura, 1971) and solar system ^{53}Mn/^{55}Mn (Trinquier *et al.*, 2008) result in only a minor shift in the model ages of generally <0.02 Myr which is insignificant. However, using a solar system initial ε^{53}Cr = −0.30, which is within its reported uncertainty (ε^{53}Cr = −0.23 ± 0.09; Trinquier *et al.*, 2008), results in a perfect fit with the mean ^{182}Hf–^{182}W model ages for magmatic iron meteorite groups (Fig. 2). Consequently, ε^{53}Cr = −0.30 is proposed as a better estimate for the solar system initial ε^{53}Cr. To maintain a match between Hf–W and Mn–Cr model ages the uncertainty on the initial ε^{53}Cr of the solar system is less than ±0.05.

Figure 3 presents a timeline depicting chromite/daubréelite model ages for IIAB, IIIAB and IVA iron meteorites and parent body metamorphism ages for type 3 and 6 ordinary chondrites as determined in Anand *et al.* (2021) using updated parameters for model age calculation. Combined with the existing thermal models (*e.g.*, Qin *et al.*, 2008), Hf–W core formation ages and calibrated Mn–Cr model ages constrain the accretion of the magmatic iron meteorite parent bodies to within less

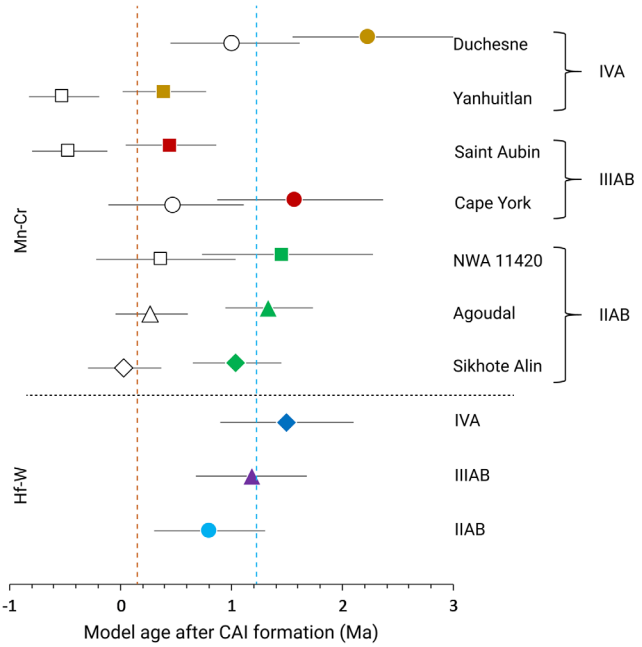

Figure 2 Comparison between Mn–Cr (present study) and Hf–W (Kruijer *et al.*, 2017) core formation ages. The Mn–Cr ages are determined using Equation 1 and ε^{53}Cr$_i$ = −0.23 (open symbols) from Trinquier *et al.* (2008) and ε^{53}Cr$_i$ = −0.30 (filled symbols) proposed in the present study.

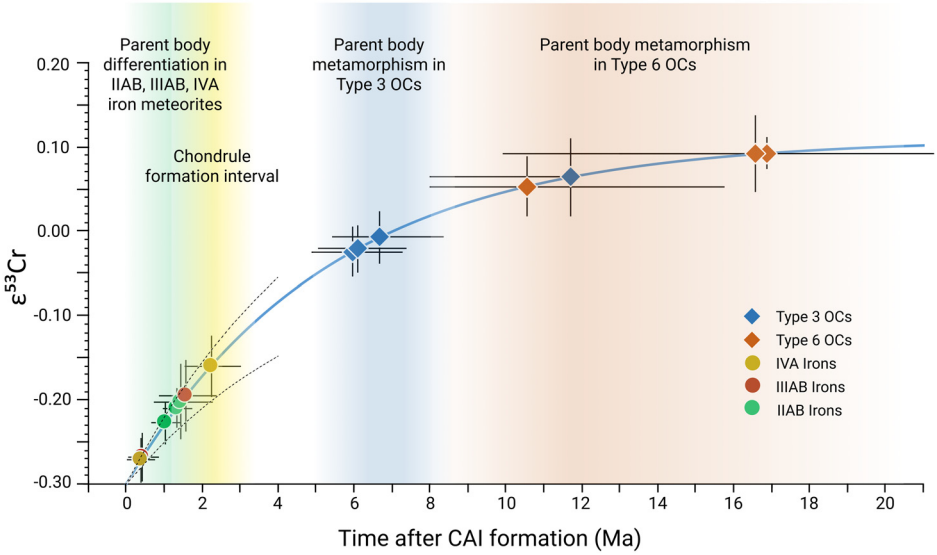

Figure 3 Timeline of early solar system formation showing parent body differentiation in magmatic iron meteorites, chondrule formation, and parent body metamorphism on ordinary chondrites (see text for references). Error envelope over iron meteorites shown by dashed lines represent the maximum variation in the evolutionary paths due to different Mn/Cr ratios of the parent bodies (see Fig. S-2).

than 1 Myr and no later than 1.5 Myr after CAI formation. This is in perfect agreement with numerical simulations that require early and efficient accretion of larger bodies within the protoplanetary disk (*e.g.*, Johansen *et al.*, 2007; Cuzzi *et al.*, 2008). The small spread in the model ages of samples from the same meteorite group might reflect some core–mantle exchange during the solidification of the metal core. The range is similar to the range of individual Hf–W model ages within an iron-meteorite group (*e.g.*, Kruijer *et al.*, 2017).

One of the most important implications of Mn–Cr and Hf–W (*e.g.*, Kruijer *et al.*, 2017; Spitzer *et al.*, 2021) core formation ages is that they bring the accretion and differentiation of the magmatic iron meteorite parent bodies in context with the chondrule formation interval recorded in chondrite samples (*e.g.*, Connelly *et al.*, 2012; Pape *et al.*, 2019, 2021). ^{207}Pb–^{206}Pb chondrule formation ages (Connelly *et al.*, 2012) suggest that the production of chondrules began as early as the CAI condensation; hence, contemporaneous with the accretion of the parent bodies of magmatic iron meteorites as suggested by Hf–W core formation ages and collaborated by Mn–Cr model ages in the present study. ^{26}Al–^{26}Mg ages for the formation of melt in individual chondrules, as summarised in Pape *et al.* (2019), suggest that chondrule formation in ordinary and most carbonaceous chondrites lasted from *ca*. 1.8–3.0 Ma with a major phase around 2.0–2.3 Ma after CAI formation. This puts the chondrule formation interval after the accretion of the magmatic iron meteorite parent bodies. The latter implies that chondrule formation may not necessarily be an intermediate step on the way from dust to planets, but rather early planet formation may have been the cause for the chondrule formation at least in extant chondrite samples. Thus, the early planetesimal formation (*i.e.* accretion of the iron meteorites parent bodies) was a local process and happened while other regions were still mostly in the stage of accreting dust particles and chondrule formation.

Acknowledgements

We appreciate the support through a 'Swiss Government Excellence Scholarship (2018.0371)' and NCCR PlanetS supported by the Swiss National Science Foundation grant no. 51NF40-141881. We thank Dr. Ludovic Ferriere from NHM Vienna for providing chromite from Saint Aubin meteorite. Dr. Harry Becker and Smithsonian Institution are thanked for providing Allende powder sample. Patrick Neuhaus and Lorenz Gfeller from the Institute of Geography, University of Bern, are thanked for assistance with the ICP-MS analysis of the samples. We thank Dr. Maud Boyet for editorial handling and Dr. Ke Zhu and an anonymous reviewer for their constructive comments that helped to improve the manuscript.

Editor: Maud Boyet

Additional Information

Supplementary Information accompanies this letter at https://www.geochemicalperspectivesletters.org/article2136.

Cite this letter as: Anand, A., Pape, J., Wille, M., Mezger, K., Hofmann, B. (2021) Early differentiation of magmatic iron meteorite parent bodies from Mn–Cr chronometry. *Geochem. Persp. Let.* 20, 6–10. https://doi.org/10.7185/geochemlet.2136

References

Amelin, Y., Kaltenbach, A., Iizuka, T., Stirling, C.H., Ireland, T.R., Petaev, M., Jacobsen, S.B. (2010) U–Pb chronology of the Solar System's oldest solids with variable ^{238}U/^{235}U. *Earth and Planetary Science Letters* 300, 343–350.

Anand, A., Pape, J., Wille, M., Mezger, K. (2021) Chronological constraints on the thermal evolution of ordinary chondrite parent bodies from the ^{53}Mn-^{53}Cr system. *Geochimica et Cosmochimica Acta* 307, 281–301.

Connelly, J.N., Bizzarro, M., Krot, A.N., Nordlund, Å., Wielandt, D., Ivanova, M.A. (2012) The absolute chronology and thermal processing of solids in the solar protoplanetary disk. *Science* 338, 651–655.

Cuzzi, J.N., Hogan, R.C., Shariff, K. (2008) Towards planetesimals: Dense chondrule clumps in the protoplanetary nebula. *The Astrophysical Journal* 687, 1432–1447.

Duan, X., Regelous, M. (2014) Rapid determination of 26 elements in iron meteorites using matrix removal and membrane desolvating quadrupole ICP-MS. *Journal of Analytical Atomic Spectrometry* 29, 2379–2387.

Goldstein, J.I., Scott, E.R.D., Chabot, N.L. (2009) Iron meteorites: Crystallization, thermal history, parent bodies, and origin. *Geochemistry* 69, 293–325.

Göpel, C., Birck, J.L., Galy, A., Barrat, J.A., Zanda, B. (2015) Mn–Cr systematics in primitive meteorites: Insights from mineral separation and partial dissolution. *Geochimica et Cosmochimica Acta* 156, 1–24.

Honda, M., Imamura, M. (1971) Half-life of Mn^{53}. *Physical Review C* 4, 1182–1188.

Johansen, A., Oishi, J.S., Mac Low, M.M., Klahr, H., Henning, T., Youdin, A. (2007) Rapid planetesimal formation in turbulent circumstellar disks. *Nature* 448, 1022–1025.

Kaminski, E., Limare, A., Kenda, B., Chaussidon, M. (2020) Early accretion of planetesimals unraveled by the thermal evolution of the parent bodies of magmatic iron meteorites. *Earth and Planetary Science Letters* 548, 116469.

Kleine, T., Budde, G., Burkhardt, C., Kruijer, T.S., Worsham, E.A., Morbidelli, A., Nimmo, F. (2020) The Non-carbonaceous–Carbonaceous Meteorite Dichotomy. *Space Science Reviews* 216, 1–27.

Kruijer, T.S., Burkhardt, C., Budde, G., Kleine, T. (2017) Age of Jupiter inferred from the distinct genetics and formation times of meteorites. *Proceedings of the National Academy of Sciences* 114, 6712–6716.

Liu, J., Qin, L., Xia, J., Carlson, R.W., Leya, I., Dauphas, N., He, Y. (2019) Cosmogenic effects on chromium isotopes in meteorites. *Geochimica et Cosmochimica Acta* 251, 73–86.

Mann, U., Frost, D.J., Rubie, D.C. (2009) Evidence for high-pressure core-mantle differentiation from the metal–silicate partitioning of lithophile and weakly-siderophile elements. *Geochimica et Cosmochimica Acta* 73, 7360–7386.

Pape, J., Mezger, K., Bouvier, A.S., Baumgartner, L.P. (2019) Time and duration of chondrule formation: Constraints from ^{26}Al–^{26}Mg ages of individual chondrules. *Geochimica et Cosmochimica Acta* 244, 416–436.

Pape, J., Rosén, V., Mezger, K., Guillong, M. (2021) Primary crystallization and partial remelting of chondrules in the protoplanetary disk: Petrographic, mineralogical and chemical constraints recorded in zoned type-I chondrules. *Geochimica et Cosmochimica Acta* 292, 499–517.

Qin, L., Dauphas, N., Wadhwa, M., Masarik, J., Janney, P.E. (2008) Rapid accretion and differentiation of iron meteorite parent bodies inferred from ^{182}Hf–^{182}W chronometry and thermal modeling. *Earth and Planetary Science Letters* 273, 94–104.

Shukolyukov, A., Lugmair, G.W. (2006) Manganese–chromium isotope systematics of carbonaceous chondrites. *Earth and Planetary Science Letters* 250, 200–213.

Spitzer, F., Burkhardt, C., Nimmo, F., Kleine, T. (2021) Nucleosynthetic Pt isotope anomalies and the Hf–W chronology of core formation in inner and outer solar system planetesimals. *Earth and Planetary Science Letters* 576, 117211.

Trinquier, A., Birck, J.L., Allègre, C.J., Göpel, C., Ulfbeck, D. (2008) ^{53}Mn–^{53}Cr systematics of the early Solar System revisited. *Geochimica et Cosmochimica Acta* 72, 5146–5163.

Wasson, J.T., Allemeyn, G.W.K. (1988) Compositions of chondrites. *Philosophical Transactions of the Royal Society of London. Series A, Mathematical and Physical Sciences* 325, 535–544.

Zhu, K., Moynier, F., Wielandt, D., Larsen, K.K., Barrat, J.A., Bizzarro, M. (2019) Timing and Origin of the Angrite Parent Body Inferred from Cr Isotopes. *The Astrophysical Journal* 877, L13.

Zhu, K., Moynier, F., Schiller, M., Alexander, C.M.O'D., Davidson, J., Schrader, D.L., van Kooten, E., Bizzarro, M. (2021) Chromium isotopic insights into the origin of chondrite parent bodies and the early terrestrial volatile depletion. *Geochimica et Cosmochimica Acta* 301, 158–186.

Geochemical Perspectives Letters

Early differentiation of magmatic iron meteorite parent bodies from Mn–Cr chronometry

A. Anand, J. Pape, M. Wille, K. Mezger, B. Hofmann

Supplementary Information

The Supplementary Information includes:

1. Samples and Analytical Methods

Seven samples from IIAB, IIIAB and IVA iron meteorite groups were analysed in this study. Chromite from whole rock iron meteorites, Sikhote Alin, Agoudal & Cape York and daubréelite from samples NWA 11420, Yanhuitlan & Duchesne (all from the Natural History Museum Bern) were separated. Pre-isolated chromite grains from sample Saint Aubin were received from the Natural History Museum Vienna. Sample collection numbers are provided in Table 1. At the University of Bern, chromite grains were identified using an optical microscope and isolated in small whole-rock fragments. The fragments were hand crushed using a pre-cleaned agate mortar and treated in conc. aqua regia on a hot plate set to 90 °C for 48 h to completely dissolve the metal-sulphide dominated matrix, leaving behind residual chromite grains. To separate daubréelite, whole meteorite fragment or troilite (sulphide) nodules were treated with conc. aqua regia at room temperature for 12 h and the residue was further separated into a magnetic and non-magnetic fraction using a magnet. Daubréelite grains were isolated from the non-magnetic portion and confirmed with energy dispersive X-ray spectroscopy (EDS) on a ZEISS EVO50 SEM. Consecutively, individual grains were handpicked. Chromite and daubréelite grains weighing 1–3 mg from all the samples were transferred to a 7 mL Savillex® vial with 150–250 mg ammonium bifluoride (ABF, $NH_4F{\cdot}HF$, Sigma-Aldrich®, Trace Metal grade) and completely digested following the protocol described in O'Hara *et al.* (2017). The sample and reagent mixture was thermalized in a convection oven set to 230 °C for 48 h. Upon cooling, the mixture was dried down twice, first after treatment with 2 mL conc. HNO_3 and then after treatment with 1 mL conc. HNO_3 and 2 mL MilliQ® water.

Before chemical separation, an aliquot from digested chromite/daubréelite fraction from each sample was diluted in 10 mL 0.5 M HNO_3 to target for a 10 ppb Cr solution. These aliquots were used to determine Cr, Mn, and Fe concentrations using a 7700x Agilent ICP-MS at the Institute of Geography, University of Bern. Uncertainties on

Mn/Cr and Fe/Cr ratios are reported as 2 s.e. of the replicate measurements (n = 5) and remained <5 % for all the samples.

The procedure for Cr purification was adopted from Schoenberg *et al.* (2016). It includes three steps of a combination of cation–anion exchange chromatography modified after Schoenberg and von Blanckenburg, (2005) (column 1), Trinquier *et al.* (2008a) and Yamakawa *et al.* (2009) (column 2 and 3). In brief, an aliquot containing 15 µg Cr from each sample was taken up in 1 mL 6 M HCl and loaded on the first 7.5 mL Spectrum® polypropylene column containing 2 mL anion resin (BioRad® AG 1X8 100–200 mesh size). The Cr eluate from the first column was dried down, redissolved in 400 µL 6 M HCl, equilibrated on a hotplate set to 130 °C for ~30 min one day before the chemical separation and stored at room temperature overnight. The next day, the sample was re-equilibrated on a hot plate at 130 °C for one hour, diluted with 2 mL MilliQ® water to obtain 2.4 mL 1 M HCl and loaded on the second column filled with 2 mL cation resin (BioRad® AG 50W-X8 200–400 mesh size). The second column separation step produced a solution with mostly Cr, but incompletely separated from Ti and V. The third column with 0.5 mL BioRad® AG 50W-X8 200–400 mesh was used in order to obtain a clean Cr separate, free of Ti and V. The elute from the second column was dried down on a hot plate (at 90 °C), taken up in 0.5 mL conc. HNO_3 and dried down again immediately to transform the samples into nitrate form. The residue was redissolved in 3 mL 0.4 M HNO_3 for 30 min on a hotplate at 80 °C and let react cold for 5 days for the production of chloro-aquo complexes. Afterwards, each sample was loaded on the third column. The matrix was eluted in 8 mL 0.5 M HF and 9.5 mL 1 M HCl, and Cr was collected in 8 mL 4 M HCl. Finally, the Cr separate was redissolved in 100 µL conc. HNO_3 and dried immediately at 130 °C on a hotplate. This step was repeated two times until the residual organics from the column chemistry was completely destroyed. Typical recovery of Cr was in excess of 80 % for the whole column chemistry, determined by measurement of spiked sample solutions on an ICP-MS. Total chemistry blanks were below 10 ng, which are negligible compared to the µg range of Cr isolated and loaded on the filaments for each sample. The purified Cr was dissolved in a sufficient amount of 6 M HCl to yield a solution with a Cr concentration of *ca.* 1 µg/µL for loading on Re filaments for mass spectrometry. 1 µg/µL Cr was mixed with 1.4 µL 4 % silica gel on a piece of Parafilm® and loaded on the filament, minimizing the spread of the sample droplet. 0.7 µL Al (1000 ppm) and 0.7 µL H_3BO_3 (5000 ppm B) was then added to the top of this mixture. After drying the mixture at around 0.8 A, the filament was heated slowly to a dull red glow for less than one second.

The samples were analysed by Thermal Ionization Mass Spectrometer using a Thermo Scientific TRITON Plus instrument at the Institute of Geological Sciences, University of Bern. Aliquots of each sample were loaded on multiple filaments and measured at ^{52}Cr signal intensity between 8 and 12 V (10^{-11} Ω resistor). Intensities of ^{50}Cr, ^{51}V, ^{52}Cr, ^{53}Cr, ^{54}Cr, ^{55}Mn and ^{56}Fe were measured on the Faraday cups L3, L2, L1, C, H1, H2 and H3, respectively (Trinquier *et al.*, 2008a). Alignment of all Cr peaks (peak scan) was ensured before each measurement and peak centre was monitored on ^{53}Cr in the centre cup. Isobaric interference of ^{54}Fe on ^{54}Cr was corrected by monitoring ^{56}Fe. The isotopes ^{49}Ti and ^{51}V were measured to correct for isobaric interferences on ^{50}Cr. However, the ^{49}Ti and ^{51}V intensities remained indistinguishable from background intensities for all samples, verifying successful separation of V and Ti from Cr during column chromatography. A typical run for a single filament consisted of 24 blocks with 20 cycles each (integration time = 8.389 s), obtained in static acquisition mode. Gain calibration was done once, at the beginning of every measurement day. Amplifiers were rotated and the baseline was measured after every block (baseline = 30 cycles, each of 1.05 s). The Cr standard reference material NIST SRM 979, was used as a terrestrial reference material. The ^{53}Cr/^{52}Cr and ^{54}Cr/^{52}Cr ratios were normalized to ^{52}Cr/^{50}Cr = 19.28323 (Shields *et al.*, 1966) by applying the exponential mass fractionation law and are reported as ε^iCr, where $\varepsilon^i\text{Cr} = ([^i\text{Cr}/^{52}\text{Cr}]_{\text{sample}} / [^i\text{Cr}/^{52}\text{Cr}_{\text{NIST SRM 979}}] - 1) \times 10^4$ and i = 53 or 54.

2. Precision and Accuracy of Cr Isotope Data

The ε^iCr (i = 53 or 54) reported for any one sample represent the mean of the replicate measurements (n = 7–13, Tables 1, S-1). The replicate measurements for each sample are used to determine the external precision reported as 2 s.e. (Tables 1, S-1). The isotope compositions of each sample are reported relative to the mean value of the standard reference material (NIST SRM 979) measured along with the samples in each measurement session (single

turret). The external precision (2 s.d.) for the standard reference material (NIST SRM 979) in each measurement session was ~0.1 for ε^{53}Cr and ~0.2 for ε^{54}Cr.

To estimate the analytical accuracy of Cr isotopic data, we evaluated the consistency of results obtained on both terrestrial standards and meteorite samples and compared to the published results. The Cr isotope data (ε^{53}Cr = 0.072 ± 0.066, ε^{54}Cr = 0.881 ± 0.120) for Allende (CV) agrees with ε^{53}Cr = 0.11 ± 0.02 and ε^{54}Cr = 0.95 ± 0.06, reported in Zhu *et al.* (2021). Cr isotope data for terrestrial rock standard IAG OKUM is also in good agreement with the Cr isotope data for terrestrial samples compiled in Zhu *et al.* (2021). Whole rock samples for an ordinary chondrite (Dergaon, H5) and Acapulcoite (RF 529) measured along with the iron meteorite chromite/daubréelite fractions are in good agreement with the literature (Zhu *et al*., 2021). Additionally, ε^{54}Cr = −0.779 ± 0.061 and ε^{53}Cr = −0.268 ± 0.029 for Saint Aubin chromite reported in the present study is in perfect agreement with ε^{54}Cr = −0.81 ± 0.08 and ε^{53}Cr = −0.28 ± 0.06 reported in Trinquier *et al.* (2007, 2008b).

3. Correction for Spallogenic Cr

Spallation reactions induced by cosmic-ray exposure (CRE) can alter ^{53}Cr/^{52}Cr and ^{54}Cr/^{52}Cr ratios in solar system objects. This alteration depends on the following parameters: (1) duration and intensity of cosmic ray exposure, (2) Fe/Cr ratio, and (3) shielding condition for any given sample/component. A particular advantage of analysing chromite and daubréelite in iron meteorites is that due to low Fe/Cr ratios in these phases, spallogenic contributions of ^{53}Cr and ^{54}Cr produced by galactic cosmic radiation (GCR) from Fe are negligible and hence no correction for spallogenic Cr is required (Trinquier *et al*., 2008b; Liu *et al*., 2019). Less suitable for dating is the iron metal of iron meteorites, because of its very high Fe/Cr combined with the typically long irradiation time in space for iron meteorites, which leads to significant production of spallogenic ^{53}Cr and ^{54}Cr that is difficult to correct for and results in high uncertainties. For instance, a Fe/Cr ratio of 0.5 (Fig. S-1b), which is typical in chromite and daubréelite would result in ε^{53}Cr and ε^{54}Cr excesses of 0.002 and 0.005, respectively, even if the CRE age for the iron meteorite is as high as 800 Ma (ε^{53}Cr and ε^{54}Cr excesses determined using equation given in Table 2 in Trinquier *et al*., 2007, and a ^{53}Cr and ^{54}Cr production rate of 2.9 × 10^{11} atoms/Ma in Fe targets from Birck and Allégre, 1985). This spallogenic ε^{53}Cr and ε^{54}Cr contribution is well within the analytical uncertainties of the Cr isotopic measurements reported here.

Liu *et al.* (2019) measured Cr isotopic composition of 16 iron meteorites belonging to different chemical groups and showed that the CRE can cause coupled excesses in ε^{53}Cr and ε^{54}Cr with a linear correlation line of ε^{54}Cr = (3.90 ± 0.03) × ε^{53}Cr. This correlation is independent of the duration and intensity of cosmic ray exposure, Fe/Cr ratio and shielding condition for any given sample/component and hence provide an alternate way to test the need for spallogenic Cr correction. Figure S-1a shows an ε^{54}Cr *vs.* ε^{53}Cr plot for the chromite and daubréelite separates from the analysed iron meteorites. The ε^{54}Cr and ε^{53}Cr values show no correlation for the analysed chromite/daubréelite fractions and corroborates to the negligible spallogenic contribution in these components.

4. Summary of $(^{53}Mn/^{55}Mn)_i$ and $\varepsilon^{53}Cr_i$

Table S-3 provides a compilation of solar system initial $(^{53}Mn/^{55}Mn)_i$ and $\varepsilon^{53}Cr_i$ reported by different methods/approaches in the literature. Shukolyukov and Lugmair (2006), Moynier *et al.* (2007) and Göpel *et al.* (2015) determined the solar system initial $(^{53}Mn/^{55}Mn)_i$ and $\varepsilon^{53}Cr_i$ by evaluating the Mn/Cr data for bulk rock carbonaceous chondrites (CC) on a ^{55}Mn/^{52}Cr *vs.* ε^{53}Cr diagram. Shukolyukov and Lugmair (2006) reported that the correlation line yields a ^{53}Mn/^{55}Mn of 8.5 ± 1.5 × 10^{-6} and initial ε^{53}Cr = −0.21 ± 0.09 at the time of Mn/Cr fractionation. Göpel *et al.* (2015) obtained a $(^{53}Mn/^{55}Mn)_i$ = 6.24 × 10^{-6} and $\varepsilon^{53}Cr_i$ = −0.15 ± 0.10 from the bulk rock CC isochron. Based on this value and with respect to the age of the solar system, the authors determined solar system initial $(^{53}Mn/^{55}Mn)_i$ = 6.8 ± 0.66 × 10^{-6} and corresponding initial $\varepsilon^{53}Cr_i$ = −0.177 (see Fig. 8 in Gopel *et al*., 2015). It is important to note that ^{55}Mn/^{52}Cr *vs.* ^{53}Cr/^{52}Cr diagram for bulk rock CC is sensitive to the choice of samples that are included into the regression calculation (Gopel *et al*., 2015; Zhu *et al*., 2021). Trinquier *et al.* (2008b) constrained $(^{53}Mn/^{55}Mn)_i$ = 6.28 ± 0.66 × 10^{-6} using an isochron based on ^{54}Cr-poor fractions of CI Orgueil and reported it as the best estimate for the solar system initial ^{53}Mn abundance. However, Zhu *et al.* (2021) reported that the ^{53}Mn–^{53}Cr correlation could be a

mixing line since chondritic components, *e.g.*, CAIs, chondrules, matrix, metal, and carbonates have different origins and time of formation. To obtain the solar system initial $\varepsilon^{53}Cr_i$, Trinquier *et al.* (2008b) back-calculated $\varepsilon^{53}Cr_i$ for a wide range of chondritic reservoirs using present-day $^{53}Cr/^{52}Cr$ and Mn/Cr ratios to the time of CAI formation and reported the average of all $\varepsilon^{53}Cr_i$ as solar system initial $\varepsilon^{53}Cr_i = -0.23 \pm 0.09$. Nyquist *et al.* (2009) used a correlation regression between initial $(^{53}Mn/^{55}Mn)_i$ and initial $(^{26}Al/^{27}Al)_i$ for solar system materials that have been analysed by both Mn–Cr and Al–Mg chronometers to determine the value of initial $(^{53}Mn/^{55}Mn)_{SS} = (9.1 \pm 1.7) \times 10^{-6}$ corresponding to the assumed $(^{26}Al/^{27}Al)_{SS} = 5.1 \times 10^{-5}$. In the present study, the solar system initial $\varepsilon^{53}Cr_i = -0.30 \pm 0.05$ is proposed after calibrating the Mn–Cr model ages for the core formation in magmatic iron meteorite to the corresponding Hf–W core formation ages. The proposed value agrees with the previously reported solar system initial $\varepsilon^{53}Cr_i$ values. Additionally, it also agrees with solar system initial $\varepsilon^{53}Cr_i = -0.34$ when $(^{53}Mn/^{55}Mn)_i = 3.16 \pm 0.11 \times 10^{-6}$ and $\varepsilon^{53}Cr_i = -0.10 \pm 0.06$ (Zhu *et al.*, 2019) determined for bulk rock angrites are calibrated against the age of the solar system.

Supplementary Tables

Table S-1 $\varepsilon^{53}Cr$ and $\varepsilon^{54}Cr$ compositions of studied samples.

						$\varepsilon^{53}Cr$			$\varepsilon^{54}Cr$		
		$\varepsilon^{53}Cr$	s.e. int.[a]	$\varepsilon^{54}Cr$	s.e. int.[a]	mean	2 s.d. ext.[b]	2 s.e. ext.[b] (*n*)	mean	2 s.d. ext.[b]	2 s.e. ext.[b] (*n*)
IIAB											
Agoudal (Chr)	AG_36_1	−0.289	0.027	−0.895	0.055	−0.210	0.081	0.023 (12)	−0.784	0.206	0.060 (12)
	AG_36_1b	−0.161	0.024	−0.875	0.051						
	AG_36_1c	−0.197	0.027	−0.761	0.054						
	AG_36_1d	−0.235	0.027	−0.947	0.056						
	AG_36_1e	−0.251	0.028	−0.849	0.057						
	AG_36_3	−0.181	0.027	−0.752	0.058						
	AG_36_3b	−0.182	0.029	−0.789	0.059						
	AG_36_4	−0.187	0.031	−0.707	0.063						
	AG_36_5	−0.257	0.036	−0.693	0.074						
	AG_53_1	−0.234	0.032	−0.805	0.069						
	AG_53_2	−0.151	0.032	−0.792	0.062						
	AG_53_3	−0.193	0.029	−0.539	0.065						
Sikhote-Alin	SA_36_1	−0.159	0.028	−0.821	0.053	−0.228	0.087	0.025 (12)	−0.923	0.177	0.051 (12)
(Chr)	SA_36_2	−0.255	0.030	−1.014	0.062						
	SA_36_3	−0.249	0.026	−0.931	0.057						
	SA_36_4	−0.189	0.025	−1.036	0.059						
	SA_36_4b	−0.178	0.026	−0.972	0.049						
	SA_36_5	−0.237	0.025	−0.842	0.052						
	SA_36_5b	−0.253	0.024	−0.966	0.050						
	SA_53_1	−0.188	0.029	−0.846	0.060						
	SA_53_1b	−0.212	0.025	−0.813	0.052						
	SA_53_2	−0.231	0.029	−1.050	0.057						
	SA_53_3	−0.325	0.046	−0.803	0.078						
	SA_53_3b	−0.256	0.030	−0.978	0.062						

Table S-1 continued

						ε^{53}Cr			ε^{54}Cr		
		ε^{53}Cr	s.e. int.[a]	ε^{54}Cr	s.e. int.[a]	mean	2 s.d. ext.[b]	2 s.e. ext.[b] (*n*)	mean	2 s.d. ext.[b]	2 s.e. ext.[b] (*n*)
NWA 11420 (Daub)	Daub_37_2	−0.161	0.029	−0.808	0.063	−0.203	0.118	0.045 (7)	−0.768	0.147	0.055 (7)
	Daub_37_3	−0.183	0.031	−0.731	0.064						
	Daub_37_4	−0.131	0.026	−0.654	0.048						
	Daub_53_1	−0.161	0.029	−0.680	0.067						
	Daub_53_2	−0.222	0.024	−0.836	0.048						
	Daub_53_3	−0.320	0.032	−0.854	0.069						
	Daub_53_3b	−0.240	0.040	−0.810	0.077						
IIIIAB Cape York (Chr)	CY_41_1	−0.164	0.030	−0.672	0.062	−0.196	0.154	0.043 (13)	−0.780	0.223	0.062 (13)
	CY_41_2	−0.188	0.034	−0.888	0.067						
	CY_41_3	−0.109	0.034	−0.588	0.072						
	CY_41_3b	−0.042	0.029	−0.692	0.059						
	CY_41_2b	−0.099	0.032	−0.859	0.057						
	CY_41_1b	−0.182	0.030	−0.870	0.058						
	CY_40_1	−0.176	0.024	−0.635	0.046						
	CY_54_1	−0.240	0.045	−0.956	0.089						
	CY_54_2	−0.293	0.046	−0.766	0.082						
	CY_54_3	−0.236	0.030	−0.789	0.060						
	CY_54_1b	−0.227	0.039	−0.802	0.067						
	CY_54_2b	−0.272	0.033	−0.700	0.066						
	CY_54_3b	−0.318	0.048	−0.923	0.084						
Saint Aubin (Chr)	S'Aub_50_1	−0.273	0.033	−0.810	0.073	−0.268	0.091	0.029 (10)	−0.779	0.193	0.061 (10)
	S'Aub_50_3	−0.242	0.039	−0.710	0.083						
	S'Aub_50_2	−0.330	0.031	−0.634	0.063						
	S'Aub_54_1	−0.249	0.032	−0.903	0.068						
	S'Aub_54_1b	−0.256	0.031	−0.880	0.068						
	S'Aub_54_2	−0.326	0.033	−0.926	0.070						
	S'Aub_54_2b	−0.221	0.033	−0.763	0.069						
	S'Aub_54_3	−0.193	0.028	−0.669	0.061						
	S'Aub_54_3b	−0.333	0.028	−0.803	0.061						
	S'Aub_54_3c	−0.255	0.029	−0.696	0.061						
IVA Yanhuitlan (Daub)	Yan _55_1	−0.192	0.030	−0.351	0.057	−0.272	0.085	0.027 (10)	−0.468	0.193	0.061 (10)
	Yan _55_1b	−0.273	0.027	−0.587	0.056						
	Yan _55_2b	−0.254	0.032	−0.529	0.065						
	Yan _55_2b	−0.285	0.032	−0.397	0.067						
	Yan _55_2c	−0.335	0.027	−0.583	0.061						
	Yan _55_2d	−0.234	0.029	−0.502	0.063						
	Yan _55_3	−0.228	0.029	−0.269	0.058						
	Yan _55_3b	−0.290	0.029	−0.509	0.063						
	Yan _55_3c	−0.307	0.028	−0.449	0.063						
	Yan _55_3d	−0.319	0.030	−0.499	0.062						

Table S-1 continued

						ε^{53}Cr			ε^{54}Cr		
		ε^{53}Cr	s.e. int.[a]	ε^{54}Cr	s.e. int.[a]	mean	2 s.d. ext.[b]	2 s.e. ext.[b] (*n*)	mean	2 s.d. ext.[b]	2 s.e. ext.[b] (*n*)
Duchesne (Daub)	Duch_55_1c	−0.144	0.038	−0.680	0.087	−0.160	0.097	0.037 (7)	−0.487	0.413	0.156 (7)
	Duch_55_1d	−0.134	0.040	−0.753	0.086						
	Duch_55_1e	−0.203	0.044	−0.674	0.103						
	Duch_55_1f	−0.092	0.046	−0.286	0.099						
	Duch_55_1g	−0.171	0.041	−0.509	0.084						
	Duch_55_1x	−0.249	0.050	−0.311	0.104						
	Duch_55_1xx	−0.127	0.045	−0.198	0.104						
Standards											
IAG OKUM	OKUM_50_1	0.046	0.032	0.140	0.067	0.020	0.159	0.065 (7)	0.083	0.270	0.110 (7)
	OKUM_50_2	0.034	0.038	0.204	0.081						
	OKUM_50_3	0.013	0.029	0.057	0.063						
	OKUM_61_1	−0.054	0.029	0.114	0.064						
	OKUM_61_1b	−0.106	0.029	−0.231	0.064						
	OKUM_61_2	0.168	0.031	0.173	0.063						
	OKUM_61_2b	0.036	0.031	0.125	0.062						
Allende (CV)[c]	All1	0.045	0.031	0.967	0.061	0.072	0.132	0.066 (4)	0.881	0.241	0.120 (4)
	All1b	0.092	0.030	0.865	0.063						
	All2	−0.014	0.027	0.691	0.054						
	All2b	0.167	0.031	1.001	0.070						
Dergaon WR (H5)	D_W_63_1	0.057	0.031	−0.547	0.069	0.117	0.078	0.039 (4)	−0.380	0.244	0.122 (4)
	D_W_63_2b	0.138	0.035	−0.399	0.081						
	D_W_63_2	0.162	0.029	−0.203	0.060						
	D_W_63_1b	0.112	0.036	−0.371	0.080						
RF 529 WR (Acap)	Acap1	0.187	0.026	−0.677	0.058	0.122	0.089	0.045 (4)	−0.698	0.170	0.085 (4)
	Acap1b	0.077	0.026	−0.741	0.058						
	Acap2	0.138	0.029	−0.572	0.067						
	Acap2b	0.083	0.030	−0.801	0.064						

[a]s.e. int.: internal error (reported as 1 s.e.) for a single filament run consisted of 24 blocks with 20 cycles each (integration time = 8.389 s).

[b]s.d. ext. and s.e. ext.: external errors of the replicate measurements reported as 2 s.d. and 2 s.e., respectively. *n* = number of replicate measurements.

[c]Allende rock standard (Smithsonian standard powder, USNM 3529, Split 18 position 1).

Abbreviations: Daub, daubréelite; Chr, chromite; WR, whole rock; Acap, Acapulcoite.

Table S-2 Weighted mean $\varepsilon^{53}Cr$ and $\varepsilon^{182}W$ of combined IIAB, IIIAB and IVA groups and corresponding Mn–Cr and Hf–W model ages.

Sample	$\varepsilon^{53}Cr$	Mn–Cr Model age (Ma)	Iron meteorite group	$\varepsilon^{182}W$	Hf–W Model age (Ma)
Agoudal	−0.210 ± 0.023		IIAB	−3.40 ± 0.03	
Sikhote Alin	−0.228 ± 0.025		IIIAB	−3.35 ± 0.03	
NWA 11420	−0.203 ± 0.045		IVA	−3.32 ± 0.05	
Saint Aubin	−0.268 ± 0.029				
Cape York	−0.196 ± 0.043				
Yanhuitlan	−0.272 ± 0.027				
Duchesne	−0.160 ± 0.037				
Weighted mean	−0.227 ± 0.006	0.03 ± 0.06[a] 1.04 ± 0.08[b]	Weighted mean	−3.37 ± 0.01	1.04 ± 0.09

Errors associated with weighted means are given in 1 s.e.
Mn–Cr model ages are determined using $\varepsilon^{53}Cr_i = -0.23$[a] and $\varepsilon^{53}Cr_i = -0.30$[b] in Equation 1 (see main text). The procedure to determine Hf–W model ages is adopted from Kruijer *et al.* (2017) and determined using the following equation and parameters:

$$\Delta t = (-1/\lambda) \times \ln [(\varepsilon^{182}W_{sample} - \varepsilon^{182}W_{chondrites}/\varepsilon^{182}W_{SSI} - \varepsilon^{182}W_{chondrites})]$$

Δt represents the time elapsed since the start of the solar system, $\varepsilon^{182}W_{sample}$ represents the pre-exposure $\varepsilon^{182}W$ of any iron meteorite group (Kruijer *et al*., 2017), $\varepsilon^{182}W_{chondrites}$ is the composition of carbonaceous chondrites (−1.91 ± 0.08) (Kleine *et al*., 2004), $\varepsilon^{182}W_{SSI}$ is the solar system initial value of –3.49 ± 0.07 as obtained from CAIs (Kruijer *et al*., 2014), and λ is the decay constant of ^{182}Hf (0.078 ± 0.002 Myr^{-1}, 2σ; Vockenhuber *et al*., 2004). A better fit between Mn–Cr and Hf–W model ages is obtained when Mn–Cr model ages are determined using $\varepsilon^{53}Cr = -0.30$.

Table S-3 Summary of $(^{53}Mn/^{55}Mn)_i$ and $(\varepsilon^{53}Cr)_i$.

$(^{53}Mn/^{55}Mn)_i$	$(\varepsilon^{53}Cr)_i$	References	Method/Approach
$(8.5 \pm 1.5) \times 10^{-6}$	−0.21 ± 0.09	Shukolyukov and Lugmair (2006)	Bulk CC isochron
$(6.53 \pm 1.93) \times 10^{-6}$	−0.23 ± 0.11	Trinquier *et al.* (2008b)	Inner solar system
$(6.28 \pm 0.66) \times 10^{-6}$		Trinquier *et al.* (2008b)	Orgueil (CI1) leachates
$(9.1 \pm 1.7) \times 10^{-6}$		Nyquist *et al.* (2009)	Best Estimate from $(^{53}Mn/^{55}Mn)_i$ *vs.* $(^{26}Al/^{27}Al)_i$
6.8×10^{-6}	−0.177	Göpel *et al.* (2015)	Bulk CC isochron calibrated against the solar system age
	−0.30 ± 0.05	This study	Proposed from combined Mn–Cr and Hf–W chronometry of IIAB, IIIAB and IVA iron meteorite groups

Supplementary Figures

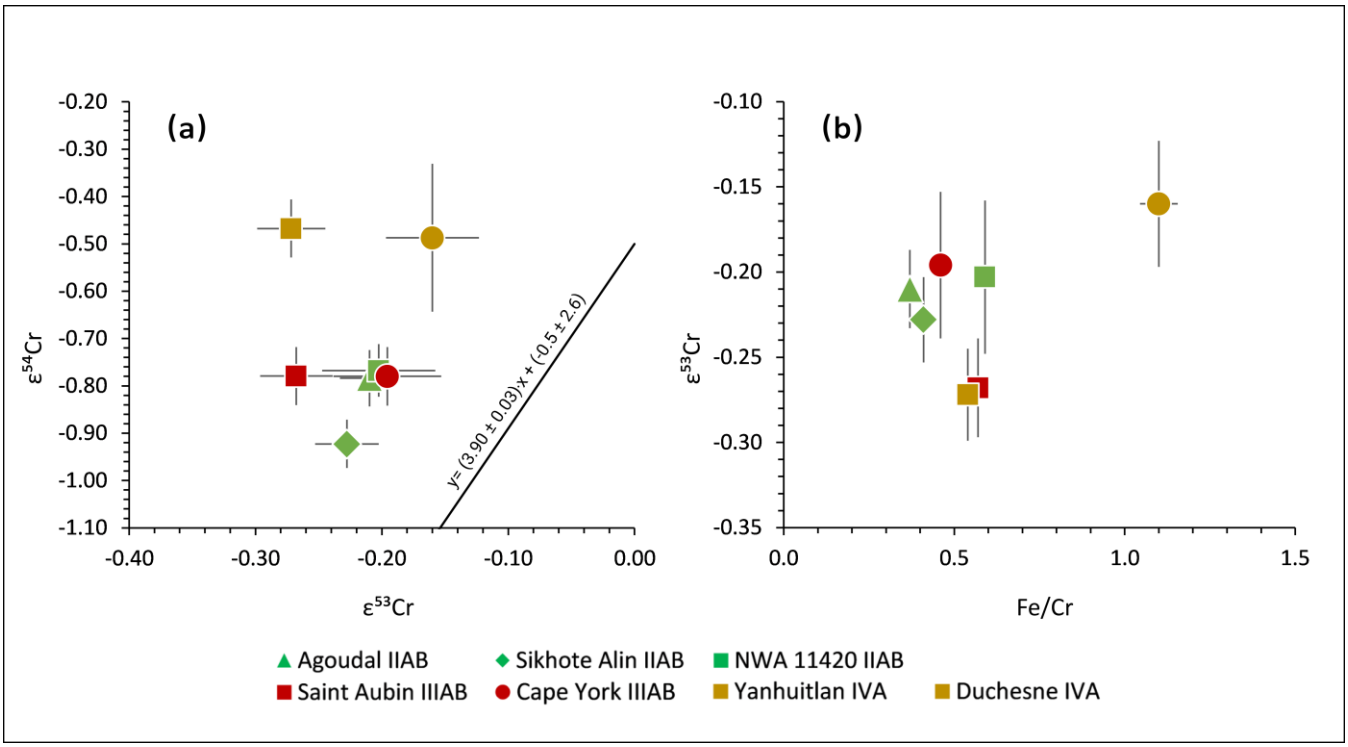

Figure S-1 **(a)** ε^{53}Cr *vs.* ε^{54}Cr and **(b)** Fe/Cr *vs.* ε^{53}Cr plots for the analysed iron meteorite samples. The black line in **(a)** shows a linear correlation between excesses in ε^{54}Cr and ε^{53}Cr [$y = (3.90 \pm 0.03)x + (-0.5 \pm 2.6)$ (95 % conf.)] determined by Liu *et al.* (2019) for iron meteorites analysed by Qin *et al.* (2010), Bonnand and Halliday (2018) and Liu *et al.* (2019). The error on the correlation line is not shown for the sake of clarity. The ε^{54}Cr and ε^{53}Cr values show no correlation for the analysed chromite/daubréelite fractions, corroborating the negligible spallogenic contribution in these components.

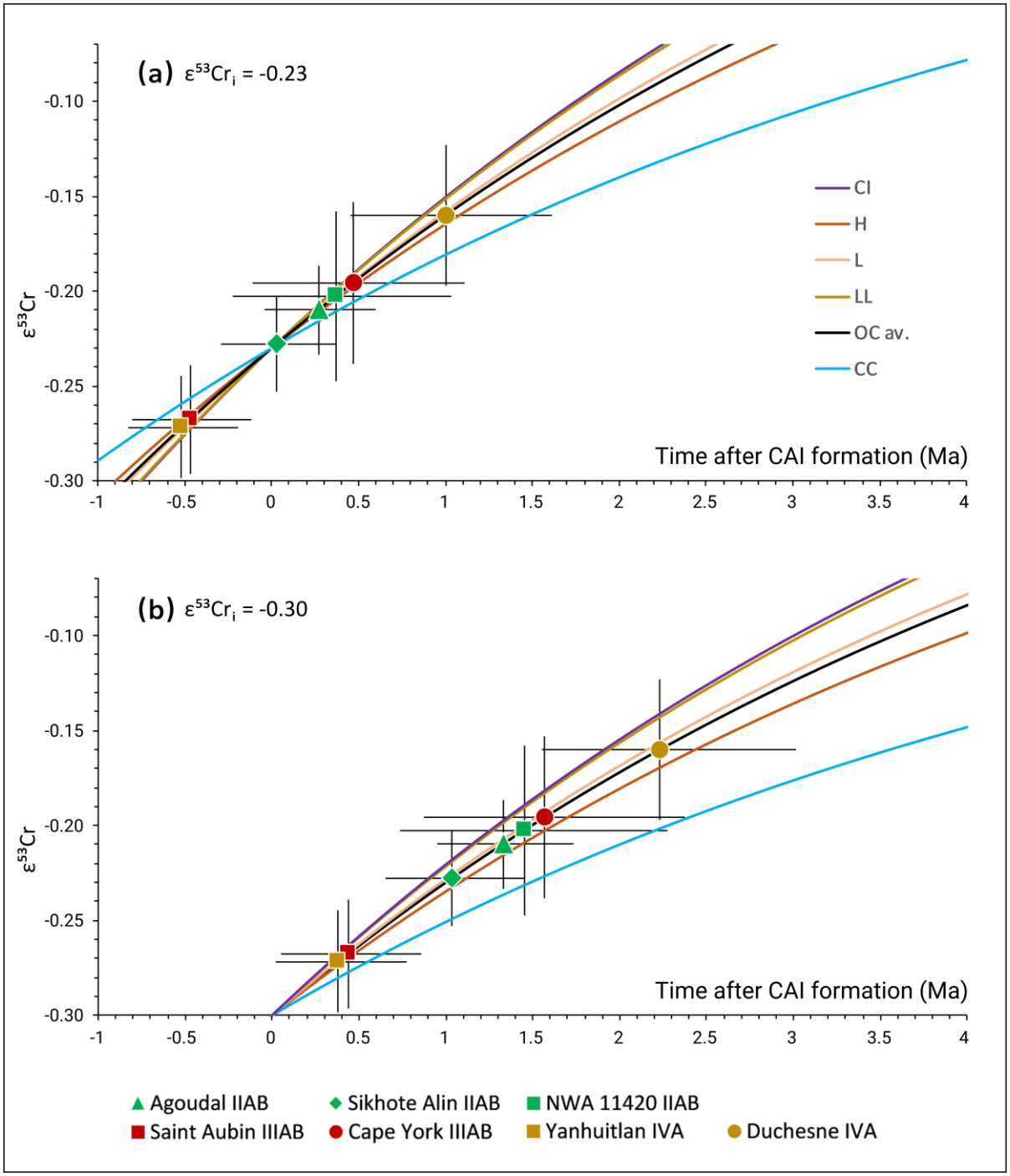

Figure S-2 Mn–Cr model ages plotted on an $\varepsilon^{53}Cr$ evolution curve using Equation 1 and solar system initial values of **(a)** $\varepsilon^{53}Cr_i = -0.23$ from Trinquier *et al.* (2008b) and **(b)** $\varepsilon^{53}Cr_i = -0.30$ as proposed in the present study (see main text for the model age calculation). Different evolutionary paths represent different Mn/Cr ratios of the parent bodies. The trajectories are derived using Equation 1 with the following Mn/Cr ratios: CI chondrites (0.84), H chondrites (0.69), L chondrites (0.76), LL chondrites (0.83), combined OCs (0.74) and combined CC chondrites (0.52) (Zhu *et al.*, 2021). Error bars represent 2 s.e. uncertainties. Model ages for IIAB, IIIAB and IVA groups are unaffected by the growth trajectory chosen, given current analytical resolution. Assuming a Mn/Cr similar to carbonaceous chondrites would change the model ages by a maximum of 1 Ma for the youngest sample. However, since all samples belong to the non-carbonaceous group, the average composition of OCs is most appropriate.

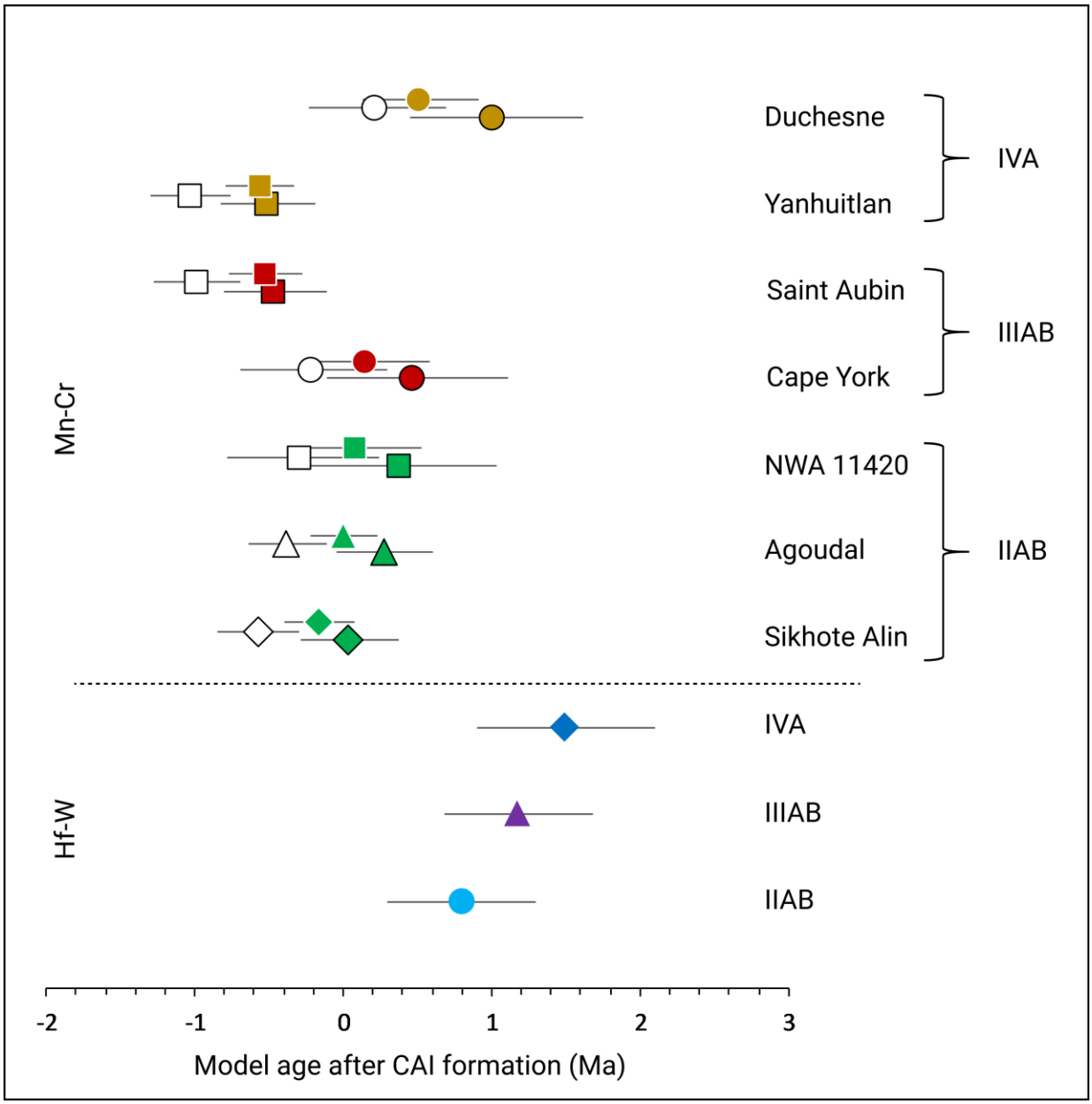

Figure S-3 Mn–Cr (present study) and Hf–W (Kruijer *et al.*, 2017) core formation ages. Mn–Cr model ages for each sample are determined using solar system initial $\varepsilon^{53}Cr_i$ and canonical $(^{53}Mn/^{55}Mn)_{ss}$ values taken from Trinquier *et al.* (2008b; coloured symbols, black borders), Göpel *et al.* (2015; coloured, no borders), and Shukolyukov and Lugmair (2006; white symbols).

Supplementary Information References

Birck, J.L., Allègre, C.J. (1985) Isotopes produced by galactic cosmic rays in iron meteorites. In: Gautier, D. (Ed.) *Isotopic ratios in the solar system*. Centre National d'Etudes Spatiales, Editions Cépaduès, Toulouse, 21–25.

Bonnand, P., Halliday, A.N. (2018) Oxidized conditions in iron meteorite parent bodies. *Nature Geoscience* 11, 401–404.

Göpel, C., Birck, J.L., Galy, A., Barrat, J.A., Zanda, B. (2015) Mn–Cr systematics in primitive meteorites: Insights from mineral separation and partial dissolution. *Geochimica et Cosmochimica Acta* 156, 1–24.

Kleine, T., Mezger, K., Palme, H., Münker, C. (2004) The W isotope evolution of the bulk silicate Earth: Constraints on the timing and mechanisms of core formation and accretion. *Earth and Planetary Science Letters* 228, 109–123.

Kruijer, T.S., Kleine, T., Fischer-Gödde, M., Burkhardt, C., Wieler, R. (2014) Nucleosynthetic W isotope anomalies and the Hf–W chronometry of Ca-Al-rich inclusions. *Earth and Planetary Science Letters* 403, 317–327.

Kruijer, T.S., Burkhardt, C., Budde, G., Kleine, T. (2017) Age of Jupiter inferred from the distinct genetics and formation times of meteorites. *Proceedings of the National Academy of Sciences* 114, 6712–6716.

Liu, J., Qin, L., Xia, J., Carlson, R.W., Leya, I., Dauphas, N., He, Y. (2019) Cosmogenic effects on chromium isotopes in meteorites. *Geochimica et Cosmochimica Acta* 251, 73–86.

Moynier, F., Yin, Q.Z., Jacobsen, B. (2007) Dating the first stage of planet formation. *The Astrophysical Journal Letters* 671, 181.

Nyquist, L.E., Kleine, T., Shih, C.Y., Reese, Y.D. (2009) The distribution of short-lived radioisotopes in the early solar system and the chronology of asteroid accretion, differentiation, and secondary mineralization. *Geochimica et Cosmochimica Acta* 73, 5115–5136.

O'Hara, M.J., Kellogg, C.M., Parker, C.M., Morrison, S.S., Corbey, J.F., Grate, J.W. (2017) Decomposition of diverse solid inorganic matrices with molten ammonium bifluoride salt for constituent elemental analysis. *Chemical Geology* 466, 341–351.

Qin, L., Alexander, C.M.O'D., Carlson, R.W., Horan, M.F., Yokoyama, T. (2010) Contributors to chromium isotope variation of meteorites. *Geochimica et Cosmochimica Acta* 74, 1122–1145.

Schoenberg, R., von Blanckenburg, F. (2005) An assessment of the accuracy of stable Fe isotope ratio measurements on samples with organic and inorganic matrices by high-resolution multicollector ICP-MS. *International Journal of Mass Spectrometry* 242, 257–272.

Schoenberg, R., Merdian, A., Holmden, C., Kleinhanns, I.C., Haßler, K., Wille, M., Reitter, E. (2016) The stable Cr isotopic compositions of chondrites and silicate planetary reservoirs. *Geochimica et Cosmochimica Acta* 183, 14–30.

Shields, W.R., Murphy, T.J., Catanzaro, E.J., Garner, E.L. (1966) Absolute isotopic abundance ratios and the atomic weight of a reference sample of chromium. *Journal of Research of the National Bureau of Standards Section A: Physics and Chemistry* 70A, 193.

Shukolyukov, A., Lugmair, G.W. (2006) Manganese–chromium isotope systematics of carbonaceous chondrites. *Earth and Planetary Science Letters* 250, 200–213.

Trinquier, A., Birck, J.L., Allègre, C.J. (2007) Widespread ^{54}Cr heterogeneity in the inner solar system. *The Astrophysical Journal* 655, 1179–1185.

Trinquier, A., Birck, J.L., Allègre, C.J. (2008a) High-precision analysis of chromium isotopes in terrestrial and meteorite samples by thermal ionization mass spectrometry. *Journal of Analytical Atomic Spectrometry* 23, 1565–1574.

Trinquier, A., Birck, J.L., Allègre, C.J., Göpel, C., Ulfbeck, D. (2008b) ^{53}Mn–^{53}Cr systematics of the early Solar System revisited. *Geochimica et Cosmochimica Acta* 72, 5146–5163.

Vockenhuber, C., Oberli, F., Bichler, M., Ahmad, I., Quitté, G., Meier, M., Halliday, A.N., Lee, D.C., Kutschera, W., Steier, P., Gehrke, R.J. (2004) New half-life measurement of ^{182}Hf: Improved chronometer for the early solar system. *Physical Review Letters* 93, 172501.

Yamakawa, A., Yamashita, K., Makishima, A., Nakamura, E. (2009) Chemical separation and mass spectrometry of Cr, Fe, Ni, Zn, and Cu in terrestrial and extra-terrestrial materials using thermal ionization mass spectrometry. *Analytical Chemistry* 81, 9787–9794.

Zhu, K., Moynier, F., Wielandt, D., Larsen, K.K., Barrat, J.A., Bizzarro, M., (2019) Timing and origin of the angrite parent body inferred from Cr isotopes. *The Astrophysical Journal Letters* 877, L13.

Zhu, K., Moynier, F., Schiller, M., Alexander, C.M.O'D., Davidson, J., Schrader, D.L., van Kooten, E., Bizzarro, M. (2021) Chromium isotopic insights into the origin of chondrite parent bodies and the early terrestrial volatile depletion. *Geochimica et Cosmochimica Acta* 301, 158–186.